Solid State Phenomena
ISSN: 1662-9779, Vol. 359, pp 53-58
doi:10.4028/p-QMO4Uo

Submitted: 2023-09-08
Accepted: 2024-08-06
Online: 2024-08-22

Prediction of Contact Resistance of 4H–SiC by Machine Learning Using Optical Microscope Images after Laser Doping

Yuki Iwaizumi[1,a], Takuma Yasunami[1,b], Keita Katayama[1,c], Yoshiaki Kakimoto[1,2,d], Daisuke Nakamura[1,e], Tetsuya Goto[3,f] and Hiroshi Ikenoue[4,g*]

[1]Kyushu University, 744, Motooka, Nishi-ku, Fukuoka, Japan, 819-0395

[2]Department of Gigaphoton Next GLP, Kyushu University, 744, Motooka, Nishi-ku, Fukuoka, Japan, 819-0395

[3]New Industry Creation Hatchery Center, Tohoku University, 6-6-10 Aramaki Aza Aoba, Aoba- ku Sendai, Miyagi, Japan, 980-0845

[4]Kochi University of Technology, 185 Miyanoguchi Tosayamadacho, Kami-shi, Kochi 782-8502, Japan

[a]iwaizumi.yuki.851@s.kyushu-u.ac.jp, [b]yasunami.takuma.166@s.kyushu-u.ac.jp, [c]katayama.keita.729@m.kyushu-u.ac.jp, [d]kakimoto.yoshiaki.124@m.kyushu-u.ac.jp, [e]dnakamura@ees.kyushu-u.ac.jp, [f]tetsuya.goto.b2@tohoku.ac.jp, [g]ikenoue.hiroshi@kochi-tech.ac.jp

Keywords: laser doping, contact resistance, machine learning, optical microscope image

Abstract. In this study, machine learning (ML) was employed to predict the electrical properties of finished devices, specifically focusing on the state of the contacts at the electrodes. The predictions are based on optical microscope images of the surface conditions, which were captured immediately following the laser doping of nitrogen atoms into 4H-SiC. The laser doping process involved varying the laser fluence from 0.4 to 4.0 J/cm^2 and using number of laser irradiation to 5, 10, 20, and 100 shots. The ML prediction was carried out in two steps. In STEP1, we classified the contact status into three types.: 1) Schottky junctions (insufficient doping), 2) Ohmic contact (good contact), and 3) Not ohmic (damage caused by laser irradiation). In STEP2, contact resistance prediction (numerical regression) was performed using the dataset predicted as an ohmic contact. As a result, we found that the three classifications in STEP1 could be predicted with a high accuracy of over 88%. Furthermore, the contact resistance prediction in STEP2 could be made with an accuracy (RMSPE: root mean square percent error) of 27.2%. Visualizing the prediction basis of numerical regression using modulus-reweighted grad-regression activation mapping (MoRAM) revealed that the ML model focused on the inside of the laser-irradiated area in the optical microscope image. The results of the scanning electron microscopy observation of the laser-irradiated area showed that ablation and residuals were generated during laser doping in that area. Consequently, it was concluded that our ML model predicted the contact resistance of the finished device taking into consideration these surface conditions. Even highly-skilled laser doping technicians have difficulty predicting the resistance values arising from the ablation and residue conditions. Based on above results, we conclude that our ML model is capable of predicting the electrical characteristics of a finished device, a task that is often considered challenging for humans.

Introduction

Laser doping has been investigated as a promising doping method for silicon carbide (SiC). Generally, the ion implantation + furnace annealing method is used as the doping technique. For SiC doping, the heat generated during the annealing process causes crystal defects in the SiC. In contrast, laser doping irradiates lasers locally and for an extremely short time, completing dopant addition and dopant activation in the same process. This reduces the impact of heat on SiC substrates and streamlines the device fabrication process. In addition, laser doping is more efficient than ion implantation for doping ultrasurface layers at higher concentrations. We focused on these distinct

features of laser doping, aiming to create high-concentration n-type 4H-SiC using this technique to minimize contact resistance in the electrode formation area of 4H-SiC devices [1,2].

In laser doping, it is necessary to identify the optimal conditions from a large number of control parameters to achieve the desired doping state. Especially for semiconductor devices, it is highly time-consuming to find the optimum conditions because it is necessary not only to evaluate physical properties, such as concentration and damage after laser doping, but also to fabricate prototypes of the devices and evaluate their electrical characteristics.

In this study, we have employed machine learning (ML) to predict the electrical properties of 4H-SiC laser-doped devices for reducing the lead-time required when developing semiconductor devices.

Experimental Methods

Device Process. The laser-doping process is illustrated in Fig. 1. First, a 100 nm thick silicon nitride (SiN) film is deposited on a SiC wafer through plasma chemical vapor deposition or CVD (Fig. 1 (a)). Next, the SiN film undergoes ablation via irradiation using a krypton fluoride (KrF) excimer laser (Gigaphoton, Inc.), and nitrogen is doped into the SiC (Fig. 1 (b)). Subsequently, the SiN film is removed using hot phosphoric acid (Fig. 1 (c)). Then, CF_4 and O_2 plasma + BHF solution treatments are used to remove residues in the laser-irradiated area (Fig. 1 (d)). To quantitatively measure contact resistance, electrodes with contact holes ranging from 5×5 to 40×40 μm^2 are formed in the laser-doped area (Fig. 1 (e)). In this study, two parameters of laser doping were varied: laser fluence (0.4~4.0 J/cm^2) and number of laser irradiation (5, 10, 20, 100 shots).

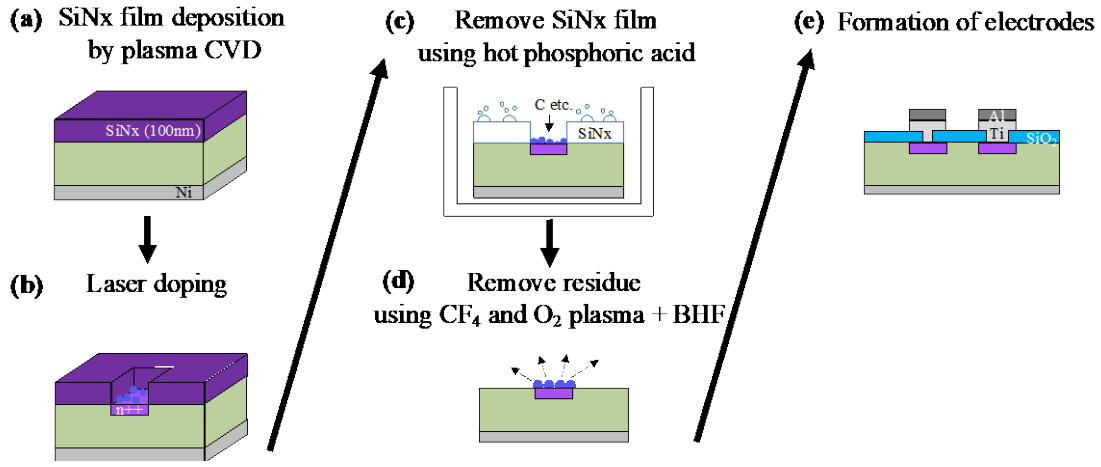

Fig. 1. Laser doping process flow.

Machine Learning (ML) Prediction. We performed laser doping under exhaustive conditions by combining laser fluence and number of laser irradiation and obtained optical microscope images immediately after laser-irradiation, which is shown in Fig. 1 (b). These image data were used as explanatory variables. We utilized the contact state of the electrode formation and contact resistance to evaluate the electrical characteristics of the device. These characteristics were used as objective variables. Our ML model was implemented using VGG16, a trained convolutional neural network model. ML prediction was performed in two steps. In STEP1, we classified all the conditions we have prepared into three types of contact states: 1) Schottky junctions (insufficient doping), 2) Ohmic contact (good contact), and 3) Not ohmic (damage caused by laser irradiation). We assembled a dataset comprising 532 images, with 380 allocated for training and 152 for validation. In STEP2, we conducted a numerical regression to predict the contact resistance based on conditions classified as ohmic. Our dataset for this step comprised 266 images, with 190 allocated for training and 76 for validation.

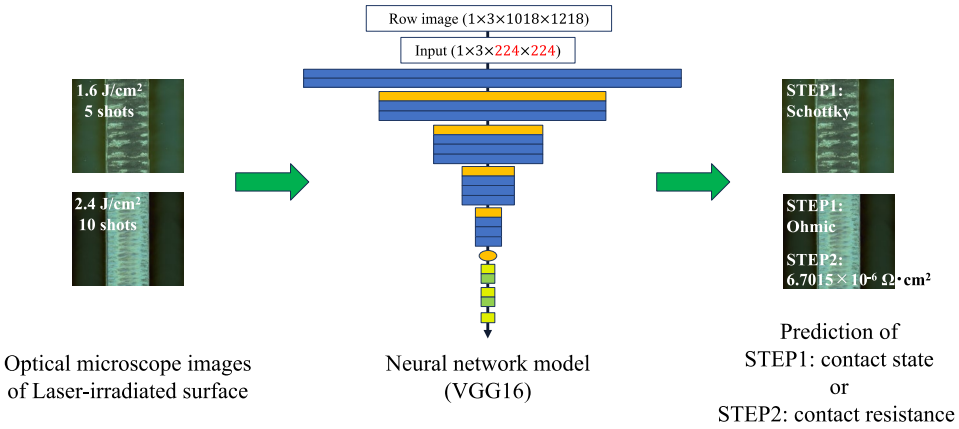

Fig. 2. Flow of the prediction process.

Visualization of ML Prediction Basis. Gradient-weighted Class Activation Mapping (GradCAM) is a technique for visualizing the basis for ML predictions in the field of image recognition [3]. This technique generates a heatmap that highlights the pixels of an input image that the ML model pays attention to, and to what extent it does so during classification prediction. In numerical regression, the decision-basis visualization technique is called regression activation mapping (RAM), with modulus-reweighted grad-RAM (MoRAM) proposed as a derivative of Grad-CAM [4]. In this study, we employed MoRAM to visualize the basis of decisions in a numerical regression.

Results and Discussions

STEP1: Three Classifications of Contact Status. Table 1 presents the classification accuracy of STEP1, which was 88% or higher for all three accuracy indices: Precision, Recall, and F-measure. Precision represents the percentage of correct predictions of the total number of predictions for a class. Recall indicates the percentage of correct predictions out of the total number of predictions for a given class and measurement. F-measure is the harmonic mean of Precision and Recall.

Table 1. Classification accuracy index

[%]	Schottky	Ohmic	Not ohmic
Precision	95	94	100
Recall	100	92	88
F-measure	97	93	94

STEP2: Contact Resistance Regression. The prediction results for STEP2 are depicted in Fig. 3. The vertical axis represents the measured values and the horizontal axis represents the predicted values. Figure 3 illustrates the correlation between the measured and predicted values, with a prediction accuracy (RMSPE: Root Mean Square Percent Error; the lower the value, the higher the accuracy) of 27.2%. Table 2 lists the measured contact resistances, numerical regression predictions, and prediction accuracies for each shot number. Table 2 indicates that the contact resistance for 5, 10, and 20 shots is in the 10^{-6} Ωcm^2 range, which is sufficiently low. In contrast, the contact resistance for 100 shots is notably worse. The RMSPE for 5, 10, and 20 shots were 28.4, 25.2, and 9.9%, respectively. Conversely, the RMSPE at 100 shots is 39.8%, signifying a lower prediction accuracy compared to lower number of irradiations. Previous experiments conducted by our research group have demonstrated that even when laser doping is performed at the fluence of the conditions that allow ohmic contact to be obtained, internal defects develop, leading to a degradation of contact resistance as the number of shots increases [2]. Since the data presented in this study comprises optical

microscopy images of the surface, they do not include information on the crystal defects formed internally. Thus, the reduced prediction accuracy is attributed to the formation of these internal defects.

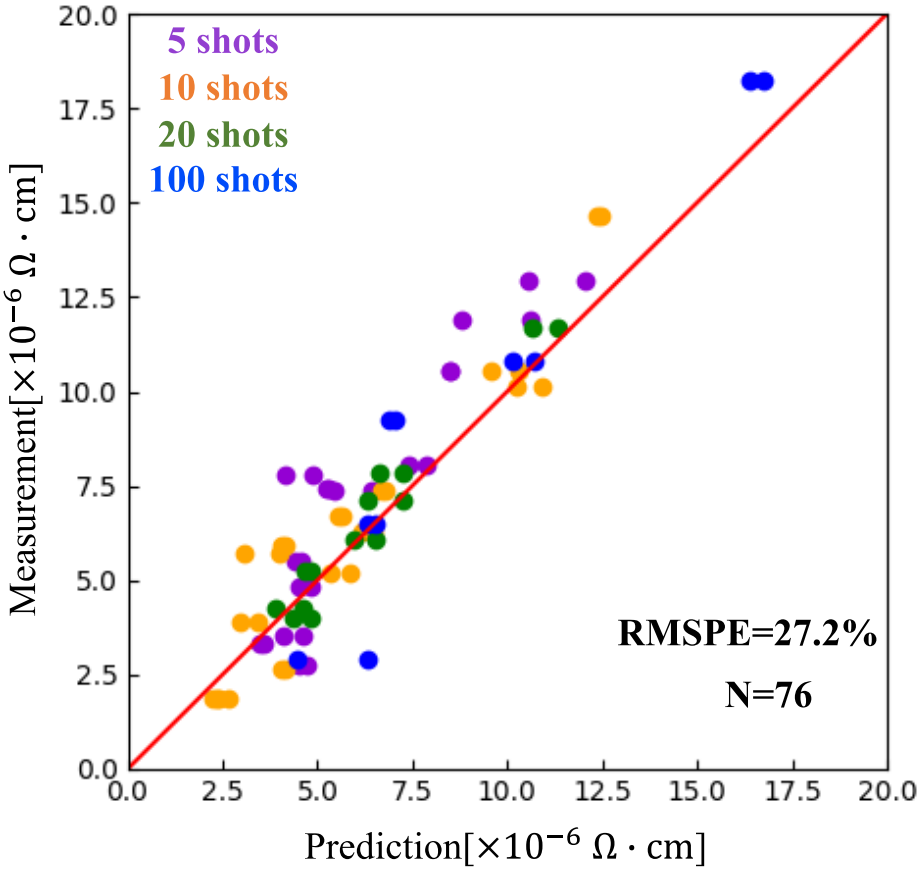

Fig. 3. Prediction result

Table 2. Measurement, prediction and RMSPE based on number of irradiations.

Number of irradiations	Measurement [×10^{-6} Ω·cm^2]	Prediction [×10^{-6} Ω·cm^2]	RMSPE [%]
5 shots	7.17 ± 3.28	6.21 ± 2.46	28.4
10 shots	6.38 ± 3.62	5.92 ± 3.18	25.2
20 shots	6.61 ± 2.55	6.36 ± 2.25	9.9
100 shots	11.42 ± 6.57	10.38 ± 4.84	39.8

Visualization of ML Prediction Basis. Figure 4 displays the optical microscope images of the laser-irradiated area utilized in STEP2, arranged by irradiation conditions (horizontal axis: fluence; vertical axis: number of irradiations). Figure 5 illustrates the results of visualization using MoRAM. Under all conditions, the ML model focused on the laser-irradiated area and the ablation pattern that appeared in it. In the 100-shots condition, the ML model placed strong emphasis on the region near the boundary between the irradiated and unirradiated areas. Furthermore, Fig. 6 showcases the optical microscopy images, MoRAM visualization results, scanning electron microscopy (SEM) images, and cross-sectional images for specific fluence conditions at 10 shots. At 1.8 J/cm^2, residue from the SiN film is evident, as confirmed by SEM images. At 2.6 J/cm^2, it is apparent that more dopants are introduced compared to 1.8 J/cm^2. Meanwhile, at 3.0 J/cm^2, the surface condition determined by SEM is not significantly different from that at 2.6 J/cm^2, but the contact resistance increased. This is attributed to defects within the crystal caused by the high fluence, which degrades the electrical conductivity. From the prediction-basis visualization and SEM observations, it is assumed that the surface conditions, such as ablation and residue on the surface, undergo changes depending on the irradiation conditions, with the ML model recognizing the changes in the surface conditions to predict the contact resistance.

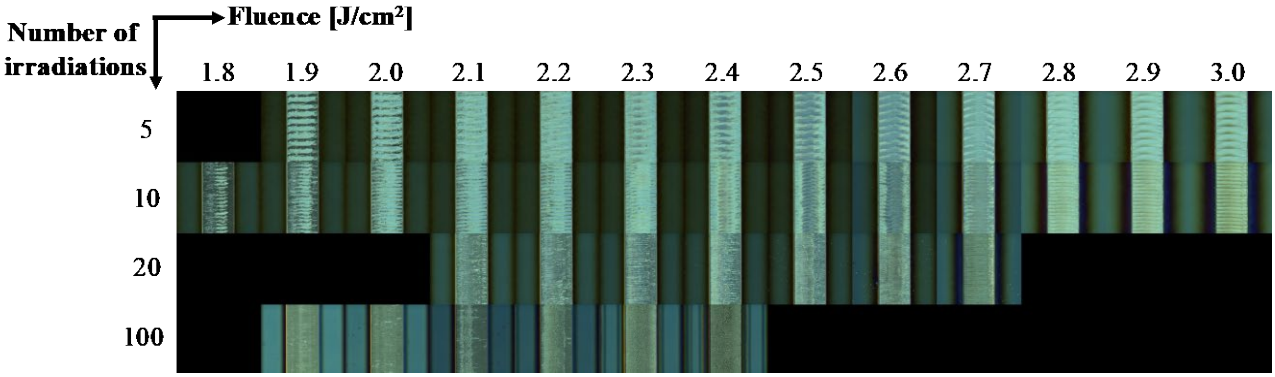

Fig. 4. Irradiated area images.

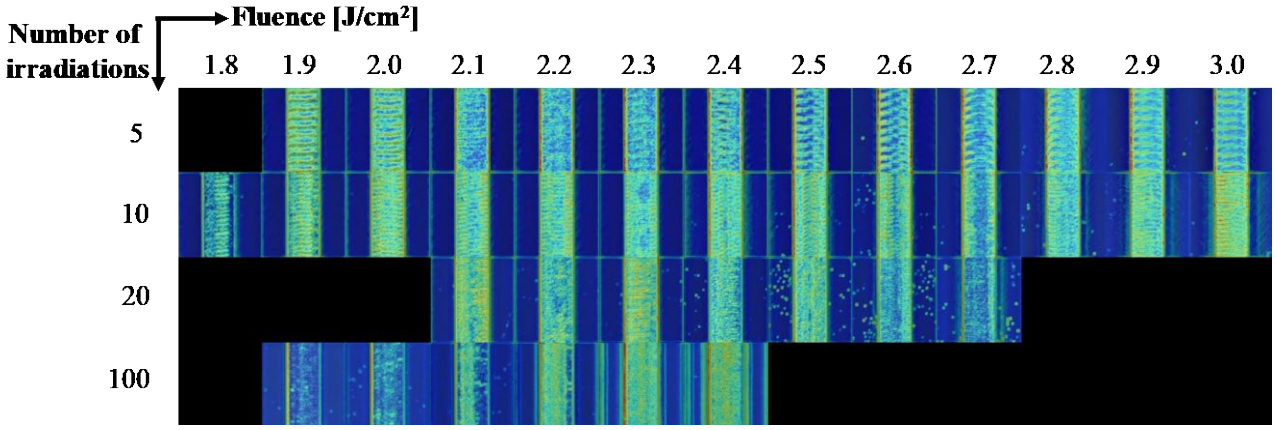

Fig. 5. Visualization result using MoRAM.

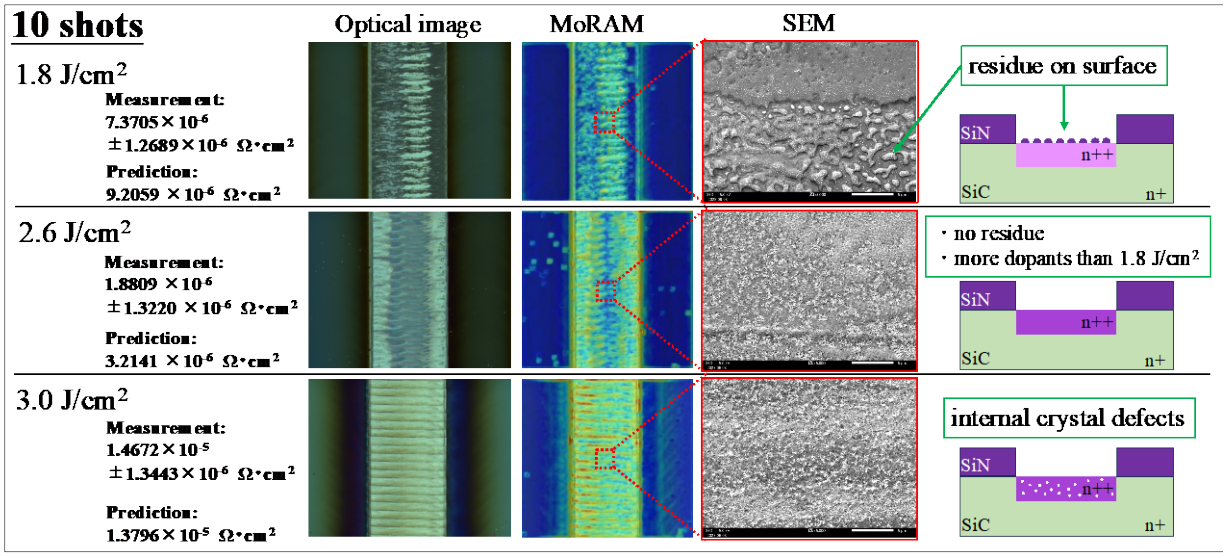

Fig. 6. Optical images, MoRAM visualization results, SEM images and cross-sectional images at partial fluence of 10shots

Conclusions

In this study, we employed ML to predict the contact state of electrode formation in the finished device using images of surface conditions immediately after laser doping. In STEP1, we conducted a three-category prediction (Schottky, Ohmic, and Not non-ohmic) and achieved an accuracy of over 88%. In STEP2, we employed numerical regression to predict contact resistance using the ohmic dataset, achieving an accuracy of RMSPE=27.2%. When the prediction basis visualization was performed using MoRAM, the ML model focused on the laser-irradiated area. As a result of

observation within the laser-irradiated area by SEM, ablation and residue material generated during laser doping was left in that area. The ML model may predict the contact resistance of the finished device from these surface conditions. Even a highly-skilled laser-doping engineer would have difficulty predicting contact resistance from ablation and residue conditions. Based on these results, we conclude that our ML model is capable of estimating the electrical characteristics of a finished device, a task that is challenging for humans to predict.

Acknowledgements

This work was supported in part by CSTI-SIP, "Photonics and Quantum Technology for Society 5.0", funding agency: QST.

References

[1] T Kikuchi et al. "Low temperature and high concentration laser doping system for fabrication of 4H-SiC power devices". Lasers in Manufacturing Conference 2021

[2] T Yasunami et al. "Laser doping mechanism of 4H-SiC by KrF excimer laser irradiation using SiNx thin films". Jpn. J. Appl. Phys. 62, SC1039 (2023).

[3] Ramprasaath R. Selvaraju et al. "Grad-CAM: Visual Explanations From Deep Networks via Gradient-Based Localization". Proceedings of the IEEE International Conference on Computer Vision (ICCV), 2017, pp. 618–626

[4] M Shimomura et al. "MoRAM: Visual Explanation of Predictive Rationale for CNN Regression Models". Information Processing Society of Japan Proceedings of the 83rd National Convention. 2021 (1), 431–432